The PEP-II B-Factory and the BABAR Detector

M.S. Witherell
Physics Department, University of California,
Santa Barbara, CA 93106-9530, USA

July 18, 1995

Abstract

I summarize the physics goals that motivate the construction of the PEP-II B-Factory and the *BABAR* detector and give a brief status report on the accelerator progress. I then describe the requirements for each of the detector systems and how the chosen design satisfies those requirements. Finally, I give projections for the physics performance.

P.A.C.S. #13.25.Hw, 11.30.Er

1 The BABAR Physics Program

With the complex phase in the CKM matrix, we have a natural explanation for *CP* violation within the Standard Model. Still, we have no convincing evidence to confirm this explanation. Providing that evidence is the primary physics goal of PEP-II and *BABAR*.

The experimental signature is the existence of *large, predictable* asymmetries in the decays of the B^0 meson to *CP* eigenstates. At *BABAR* it will be possible to make precise measurements of these CP-violating asymmetries in many different channels. In a number of other important areas, the physics from *BABAR* will be at the level of the best in the world, including measurements of CKM elements in B decays. searches for rare B decays, and charm, tau, and two-photon physics.

Years of experience have shown us the advantages of studying B decays with an e^+e^- collider with energy tuned to the $\Upsilon(4S)$.

1. The $B^0\overline{B}^0$ cross section is large ($\sigma = 0.5$ nb).
2. There are no extra fragmentation hadrons.
3. The B^0 is almost at rest in $\Upsilon(4S)$ rest frame.
4. The $B^0/\overline{B}^0$ pair remains in a $B^0/\overline{B}^0$ state (even though each meson is mixing) until one decays.

To do a definitive *CP* experiment, we need a large sample of B^0 decays, small backgrounds (branching ratios for *CP* eigenstate modes $\approx 10^{-5}$), and a way to tag the flavor of the B^0 cleanly with high efficiency. The strategy for studying *CP* violation at PEP-II is to select events in which one B decays to a *CP* eigenstate and the other decays into a mode which produces a unique tag of its flavor. If t_1 is the proper decay time of the tagging mode, and t_2 is the proper decay time of the *CP* eigenstate mode, then the time distribution is given by the expression

$$\frac{dN}{dt} \propto e^{-(t_1+t_2)/\tau}\left[1 \pm \sin(2\beta)\sin(x(t_2-t_1)/\tau)\right].$$

where the two signs correspond to even and odd CP eigenstates. Note that the asymmetry integrates to zero! That is why the relative decay time must be measured.

The need to measure the relative decay time is what drives the construction of asymmetric B-Factories at SLAC and KEK. With a 3.1 GeV beam and a 9.0 GeV beam, the center of mass energy is still 10.58 GeV, but the Bs are moving in the lab with $v \approx 0.5c$. This corresponds to an average separation of $\gamma\beta c\tau = 250\,\mu$m between the two B vertices, as shown in figure 1.

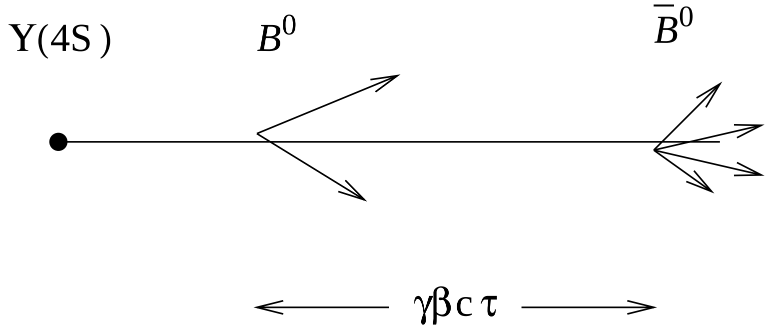

Figure 1: The separation of the two decay vertices.

2 PEP-II

The PEP-II B-Factory is being constructed by a collaboration of SLAC, LBL, and LLNL on the SLAC site. [1] There are going to be two storage rings in the PEP tunnel, a high energy ring (HER) for electrons and a low energy ring (LER) for positrons. The existing linac serves as an injector, and new bypass lines are being built for injection into the PEP-II rings.

Besides the asymmetry in the energies of the two beams, the most notable feature of the PEP-II design is the high luminosity, $3.0 \times 10^{33}\,\mathrm{cm}^{-2}\,\mathrm{s}^{-1}$. This is to be obtained by filling the two rings with a large number of bunches, with about 4 ns spacing between bunches. The parameters for PEP-II are shown in the table I.

Parameter	HER	LER	Units
Center-of-mass energy	10.580		GeV
Peak Luminosity	3.0×10^{33}		$\mathrm{cm}^{-2}\,\mathrm{s}^{-1}$
Luminosity lifetime	1.55		hr
Bunch spacing	1.26		m
Circumference	2219		m
Beam energy	9.00	3.11	GeV
Bunch length	1.0	1.0	cm
Number of bunches	1658	1658	
Particles per bunch	2.7×10^{10}	5.9×10^{10}	
Beam current	0.99	2.14	Amps
Horizontal IP spot size	155	155	μm
Vertical IP spot size	6.2	6.2	μm

Table I: PEP-II Parameters

The construction for PEP-II is matching its fast schedule. All components for the bypass lines and the electron extraction lines are ready, and the installation will be complete by August, 1995. The magnets for the HER are the original PEP magnets, which have all been refurbished and are now being measured. The installation of the magnets and redressing of the power cables has begun. The HER vacuum chamber consists of copper extrusions bent to match the curvature of the machine. They are now undergoing e-beam welding.

The LER quadrupole and dipoles magenets are new, and have been ordered from IHEP, Beijing. A prototype 1.2 MW klystron is being tested now, and eight have been ordered from industry. A 500 kW radiofrequency window is also under test, as is the first rf cavity. Eight such cavities are being fabricated at LLNL.

The PEP-II commissioning plan calls for phased commissioning, to allow a period of learning the behavior of parts of the new machine while other parts are under construction. In fall 1995, it will be possible to test the beam extraction and transport. The HER construction will be complete in summer 1997, and it will be possible to start to inject into the ring and work toward stored beam. The LER will reach a similar period of commissioning in spring 1998, and beam-beam collisions will be possible in summer 1998. BaBar will then move onto the beam line in spring 1999 and physics collisions will begin.

3 Detector Requirements

The three primary experimental goals of the BaBar detector are [2]

1. to reconstruct exclusive CP final states efficiently and cleanly;
2. to tag the flavor of the other B with high efficiency and low probability of error; and
3. to measure the relative time of the two decays.

Each of these goals puts specific demands on the detector.

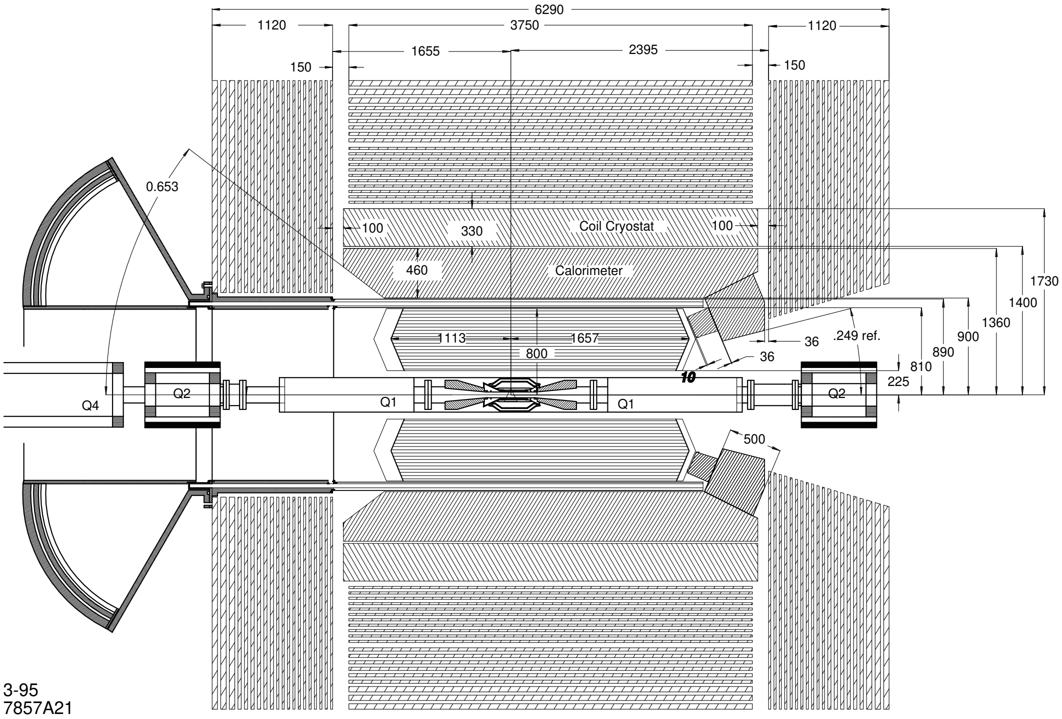

Figure 2: Cross-sectional view of the BABAR detector.

Efficient reconstruction of exclusive CP final states requires large acceptance for charged particles and neutrals, especially in the direction of the boost. It also requires very good efficiency and resolution for charged tracks down to $p_t = 50\,\mathrm{MeV}/c$ and for photons down to

$E = 20\,\text{MeV}$. Finally, identification of hadrons up to the kinematic limit from B decay is important for many of the important modes. Tagging the flavor is done with any combination of primary leptons from $\overline{B}^0 \to \ell^- X$; secondary leptons from $\overline{B}^0 \to DX$, $D \to \ell^+ Y$; and kaons from $\overline{B}^0 \to DX$, $D \to K^- Y$. Taken together, tagging requires good hadron and lepton identification down to low momentum. Measuring the relative decay time requires a vertex detector with precise z measurement. Figure 2 shows a cross sectional view of the *BABAR* detector. I will step through the main detector systems and describe their design.

The silicon vertex tracker (SVT) is more central to the *BABAR* detector than for any previous collider detector. Unless one can measure the time dependence of the *CP* asymmetry, there is no reason to build PEP-II. Also, there is no other tracking until the drift chamber, which starts at a radius of about 23 cm.

The SVT must provide precise measurements of the track position near the interaction point; the measurements of θ and ϕ ; and good efficiency for tracks with $p_{\rm t} < 100\,\text{MeV}/c$. As shown in figure 3, it consists of 5 layers of double-sided, AC-coupled silicon strip detectors. The readout pitch in inner layers is $50\,\mu$m in ϕ, $100\,\mu$m in z with one floating strip. The readout electronics use a custom rad-hard IC and time-over-threshold analog readout. The mechanical support includes very little material in the active tracking region. All electronics and cooling are outside of the tracking region.

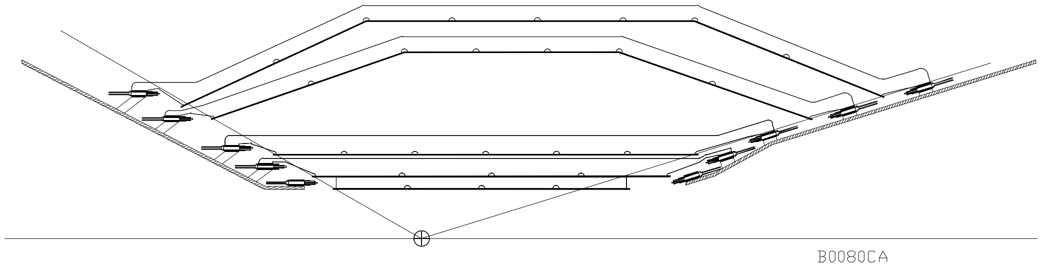

Figure 3: The Silicon Vertex Tracker. The outer layer is at a radial distance of about 14 cm from the beam.

The impact parameter resolution for a single track is $\sigma_{xy}, \sigma_z \approx 50\,\mu\text{m}/p \oplus 15\,\mu$m and the angle resolution is $\sigma_\phi, \sigma_\theta \approx 1.6\,\text{mr}/p$. Both of these resolutions are given for tracks at normal incidence. The z vertex resolution for CP eigenstates typically has about 90% in a Gaussian with $\sigma \approx 40\,\mu$m. The resolution in $\Delta z \equiv z_{CP} - z_{tag}$ is dominated by the tagging resolution, with a typical resolution on Δz of about $100\,\mu$m. The vertex resolution is dominated by multiple scattering, and the simulation should be very reliable.

For clean modes, such as $B^0 \to J/\psi K^0_S$, the resolution in Δz should be significantly less than the mean separation of 250 μm. With the detector resolution obtainable with the SVT, the CP measurement is degraded by less than 10% compared to a similar measurement with perfect vertex resolution. For modes with backgrounds, such as $B^0 \to \rho^+\pi^-$, the background is much reduced at the Δz values important for the asymmetry measurement. This is demonstrated in figure 4, which shows the Δz distribution for this case. There is a large background, but it is sharply peaked at $\Delta z = 0$, and therefore it contributes rather little at $|\Delta z| \approx 400\,\mu$m, the region most sensitive to the asymmetry.

The drift chamber and the silicon vertex tracker together form the tracking system for *BABAR*. In the compact space of $23\,\text{cm} < r < 80\,\text{cm}$, the drift chamber must provide excellent momentum resolution for charged particles with $100\,\text{MeV}/c < p_t < 2.5\,\text{GeV}/c$; full acceptance and good resolution even for very forward tracks; very good pattern recognition capability, even at high machine background; dE/dx measurement capability; and fast information for Level 1 tracking trigger.

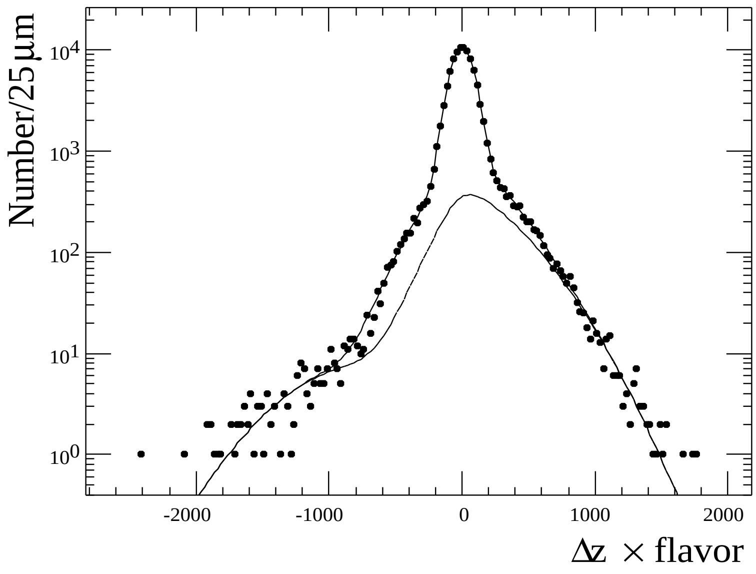

Figure 4: Δz for $B^0 \to \rho^+\pi^-$. For $\overline{B}^0$ decays, $-\Delta z$ is plotted, so that the CP asymmetry is reflected in a left-right asymmetry in the plot. The lower solid curve shows the signal, the upper curve includes background.

The main design choices to obtain the needed resolution are a 1.5 T field and a He-based gas. The drift chamber configuration is shown in figure 5. A small drift cell design is used to obtain the needed pattern recognition efficiency. There are ten superlayers, each containing four layers, with an alternating arrangement of axial and stereo superlayers. A truncated cone shape for the endplates makes it possible to achieve the necessary strength with less material. The most unusual feature of the chamber is the offset of the chamber center relative to the position of the interaction point, such that at the radius of maximum length the chamber covers the region $-1.11\,\mathrm{m} < z < 1.66\,\mathrm{m}$. All readout electronics and HV are mounted on the backward endplate to keep the material in the forward direction to a minimum.

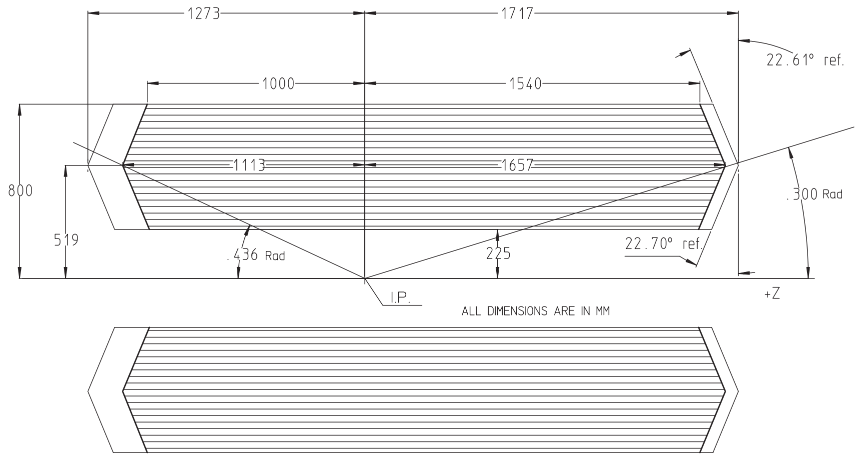

Figure 5: The drift chamber configuration. The boost direction is to the right.

The primary measure of drift chamber performance is the momentum resolution, which is shown in figure 6. The resolution at $\cos\theta_{\rm lab} = 0$ can be parameterized as $\sigma(p_{\rm t})/p_{\rm t} \sim [0.21\% + 0.14\% \times p_{\rm t}]$. The constant term is the contribution from multiple scattering, and its low value is due to He-based gas. The resolution is reasonably flat in $\cos\theta_{\rm cm}$ due to the offset of the chamber center.

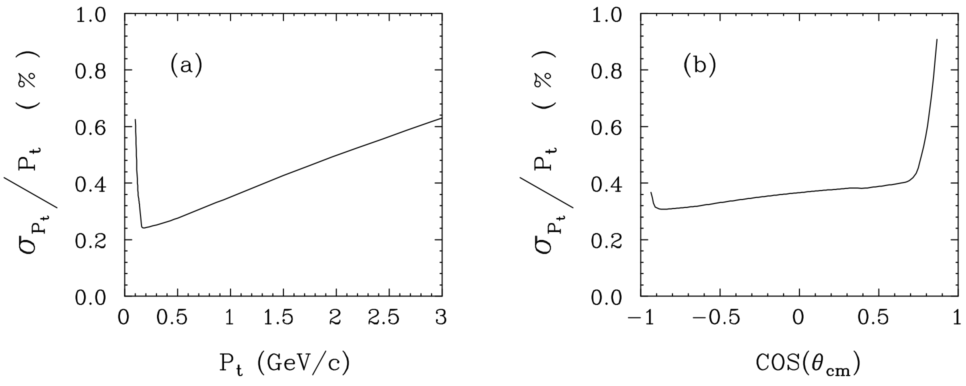

Figure 6: The resolution $\sigma(p_t)/p_t$ as a function of (a) p_t for $\cos\theta_{\rm lab} = 0$ and (b) $\cos\theta_{\rm cm}$ for $p_t = 1.0\,{\rm GeV}/c$

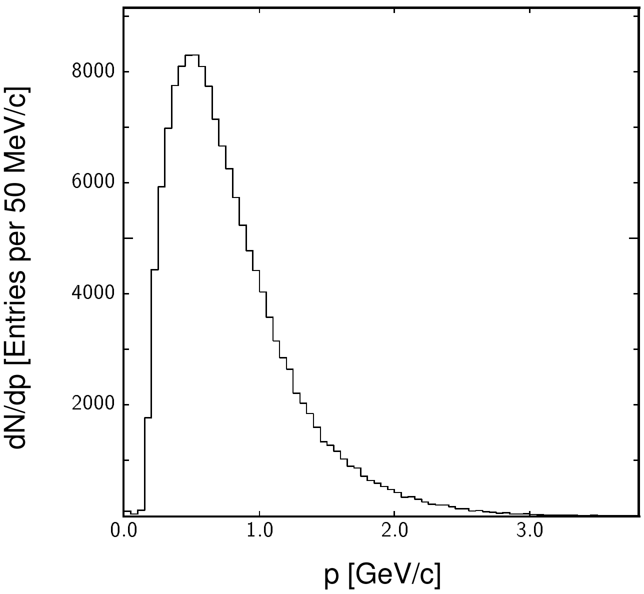

Figure 7: The momentum spectrum for kaons from B Decay.

The primary goals for hadron identification are: to identify charged kaons for tagging the other B; to reduce the backgrounds for modes such as $B \to D^+D^-$; and to help separate $B^0 \to \pi^+\pi^-$ from $B^0 \to K^+\pi^-$, etc. The momentum spectrum for kaons from B decay, relevant for the first two of these goals, is shown in figure 7. It is a fairly soft spectrum, with most of the particles having momentum less than about 1.5 GeV/c.

The pions from the decay $B^0 \to \pi^+\pi^-$ are at the kinematic limit: They range from 1.6 GeV/c backward to 4.0 GeV/c forward. If one pion from this decay is in the backward endcap region, the other one is beyond the forward acceptance, so there is no reason to have a device dedicated to hadron identification in the backward region.

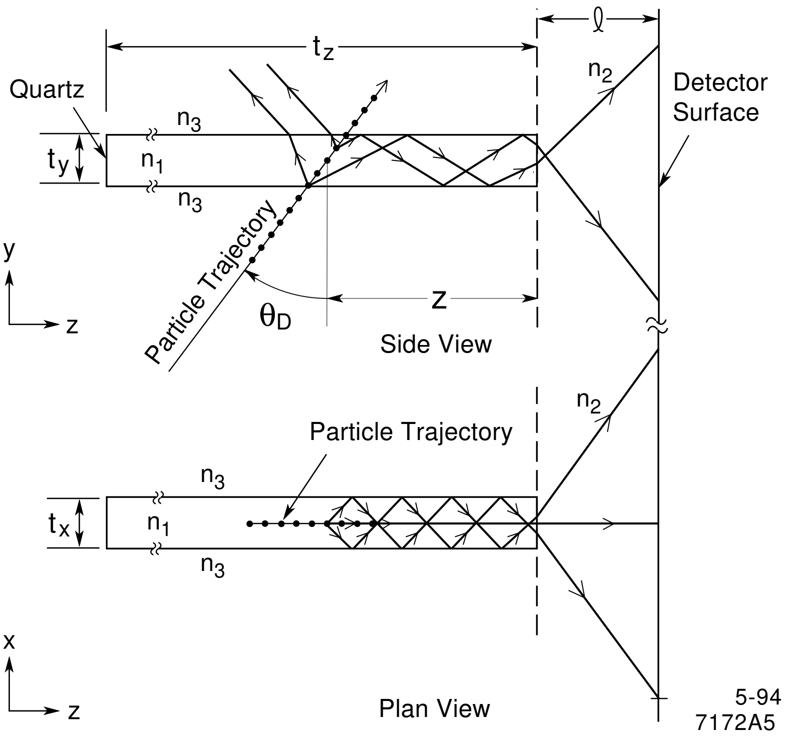

Figure 8: The principle of the DIRC

To obtain good identification at the kinematic limit requires a Cherenkov-based technique. We have chosen a DIRC (Detector of Internally Reflected Cherenkov light) in the barrel region and an ATC (Aerogel Threshold Cherenkov) counter in the forward endcap region. The DIRC principle is shown in figure 8. The particle radiates in a 1.75 cm thick quartz bar. The internally reflected light is transmitted to the end, preserving the angle information. The light exits the quartz bar into a large water tank, producing an arc of light at the outside. An array of 13,400 phototubes with 2.9 cm diameter detects the light.

The photoelectron yield is very high in the DIRC, with from 20 to 50 photoelectrons at various angles. If for some reason fewer are observed, the resolution goes like $1/\sqrt{N}$, with no sharp cutoff in efficiency due to pattern recognition. The most important quantitative measure of the DIRC performance is the significance of the K/π separation, shown in figure 9. The separation is very high at low momentum, dropping to lower values at higher momentum. The separation is always $> 4\sigma$ within the kinematic limits for particles from B decays, as can be seen from figure 10. In the forward endcap, the ATC system provides efficient identification at the kinematic limit, and very good identification of hadrons is obtained throughout the kinematic range.

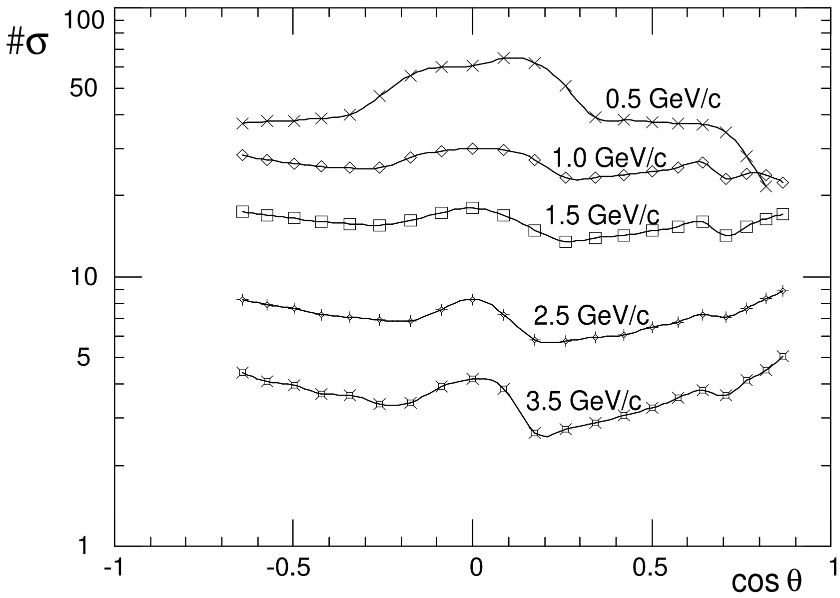

Figure 9: The K/π separation by the DIRC in standard deviations (σ) as a function of track momentum and $\cos\theta$.

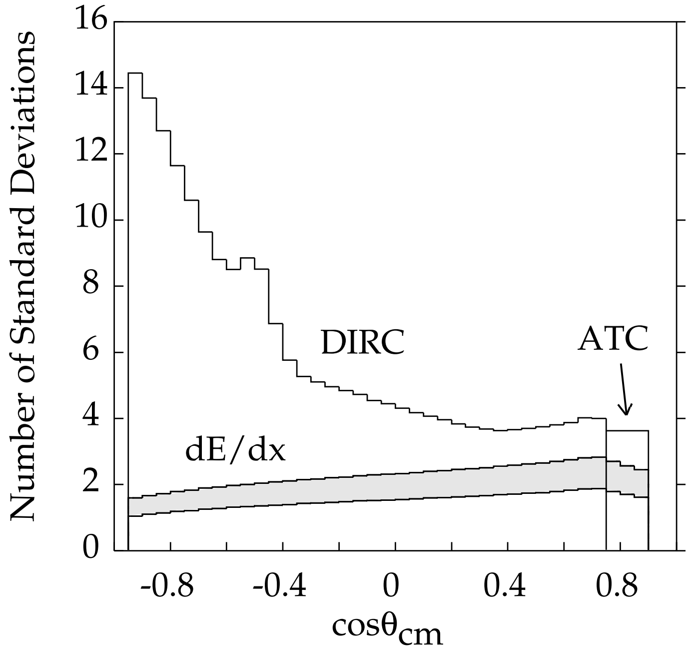

Figure 10: K/π separation for π's from $B^0 \to \pi^+\pi^-$

The primary physics objectives for the electromagnetic calorimeter are: to detect π^0s with very high efficiency and low background for CP decay modes such as $B^0 \to J/\psi K^0_S$, $K^0_S \to \pi^0\pi^0$, $B^0 \to D^{*+}D^{*-}$, and $B^0 \to \rho^+\pi^-$, $\rho^+ \to \pi^+\pi^0$; to identify electrons down to 500 MeV/c; to supplement the information from the IFR (see below) for muons and K^0_Ls; and to provide information for the neutral trigger. Figure 11 shows the photon energy spectrum for an important *CP* mode. This shows the large dynamic range over which the calorimeter must operate. Although the photons extend to an energy of 4 GeV, the most common are around 100 MeV.

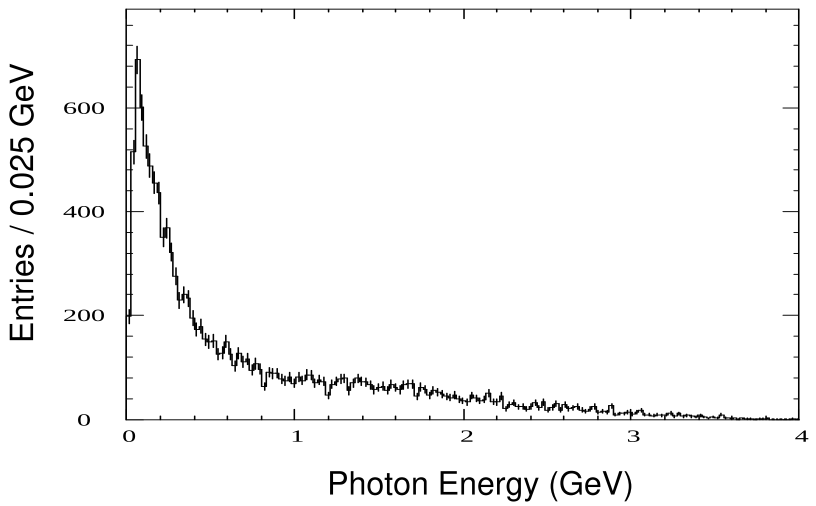

Figure 11: Photon energy spectrum from $B^0 \to \rho^+\pi^-$, $\rho^+ \to \pi^+\pi^0$

The barrel calorimeter covers the angular range $-0.80 < \cos\theta < 0.89$; the forward endcap calorimeter extends the forward acceptance, covering $0.89 < \cos\theta < 0.97$. Together there are 6480 crystals ranging from $16.0 - 17.5\ X_0$, for a total of $5.9\,\mathrm{m}^3$ of CsI. The crystals are typically about $4.8\,\mathrm{cm} \times 4.7\,\mathrm{cm}$ at the front face, and there are two independent photodiodes for each crystal.

The energy resolution for photons is $\sigma_E/E = 1\%/E(\,\mathrm{GeV})^{\frac{1}{4}} \oplus 1.2\%$, and the angular resolution is $\sigma_\theta = 3\,\mathrm{mr}/\sqrt{E(\mathrm{GeV})} \oplus 2\,\mathrm{mr}$. The $B^0 \to \rho\pi$ decay mode may be superior to $B^0 \to \pi^+\pi^-$ for measuring $\sin 2\alpha$, and is an important benchmark of calorimeter performance. The CsI calorimeter provides π^0 detection with good efficiency and low background over the entire energy range. Studies show that both energy and angular resolution are important in reducing backgrounds for this mode.

As can be seen from figure 2, the magnet iron is segmented and instrumented with chambers. The primary experimental goals of the instrumented flux return (IFR) are to reduce the lower momentum limit for detecting muons to about 0.6 GeV/c and to detect $B^0 \to J/\psi K^0_L$. The detectors are Resistive Plate Chambers (RPCs), which are being used in many existing experiments.

Figure 12 shows the momentum spectrum for leptons used to tag the flavor of the neutral B meson. There is a momentum-polar angle correlation, due to the boost. Both direct and indirect leptons are useful for tagging. Identifying low-momentum electrons using the CsI calorimeter is relatively straightforward, but it is necessary to use segmented iron to extend the muon efficiency below about 1.5 GeV/c. With the IFR, it extends down to 0.6 GeV/c.

The electronics system for BaBar accepts signals from 6 detector systems for 2.5×10^8 crossings/sec and converts them into approximately 100 events/sec for archival storage.

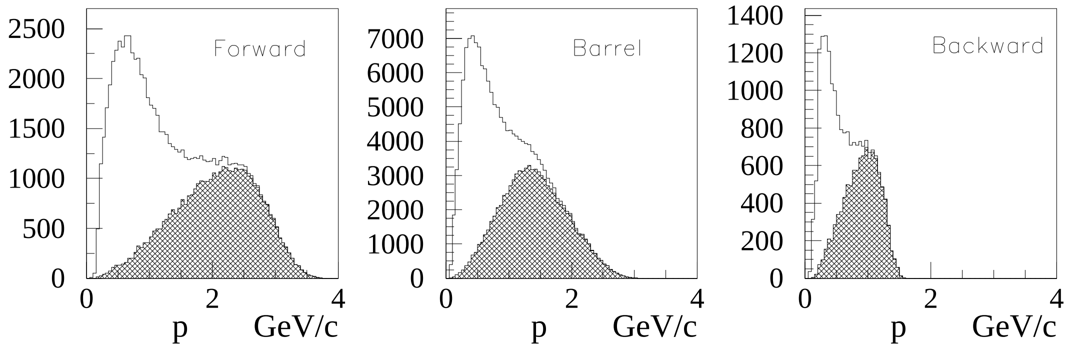

Figure 12: Lepton energy spectrum from B decay. The hatched histogram shows primary leptons from $B^0 \to \ell^+ X$. The clear shows secondary leptons from $B^0 \to \overline{D}X$, $\overline{D} \to \ell^- Y$.

Its chief features are:

1. a 2-level trigger and data acquisition architecture;
2. ful buffering in both the trigger and data flow paths;
3. nearly deadtime-free operation up to 10$\times$ nominal backgrounds;
4. standardized DAQ module design;
5. extensive use of commercial equipment; and
6. a standard software environment from DAQ module to offline computing.

Table II shows a summary of the parameters for the BABAR detector.

Detector	Technology	Dimensions	Performance
SVT	Double-Sided	5 Layers $r = 3.2 - 14.4\,\mathrm{cm}$ $-0.87 < \cos\theta < 0.96$	$\sigma_z = 50\,\mu\mathrm{m}/p_\mathrm{t} \oplus 15\,\mu\mathrm{m}$ $\sigma_\phi = \sigma_\theta = 1.6\,\mathrm{mr}/p_\mathrm{t}$
DC	Small Cell	40 Layers $r = 22.5 - 80.0\,\mathrm{cm}$ $-111 < z < 166\,\mathrm{cm}$	$\sigma(p_\mathrm{t})/p_\mathrm{t} =$ $[0.21\% + 0.14\% \times p_\mathrm{t}]$
PID	DIRC	$1.75 \times 3.5\,\mathrm{cm}^2$ quartz $-0.84 < \cos\theta < 0.90$	$N_{pe} = 20 - 50$ $\gtrsim 4\sigma K/\pi$ for all B decay products
PID	ATC	n=1.0065, 1.055 $0.916 < \cos\theta < 0.955$	$N_{pe} = 10$ π/K up to $4.3\,\mathrm{GeV}/c$
CAL	CsI(Tl)	$16 - 17.5\ X_0$ $\sim 4.8 \times 4.8\,\mathrm{cm}$ crystals	$\sigma_E/E = 1\%/E^{\frac{1}{4}} \oplus 1.2\%$ $\sigma_\theta = 3\,\mathrm{mr}/\sqrt{E} \oplus 2\,\mathrm{mr}$
MAG	SC Coil Seg. Iron	IR=1.40 m L = 3.85 m	$B = 1.5\,\mathrm{T}$
IFR	RPC	16–17 Layers	$\epsilon_\mu > 90\%$ for $p_\mu > 0.8\,\mathrm{GeV}/c$

Table II: Detector Parameter Summary

4 Physics Sensitivity

The sensitivity to the CP violation in B^0 decays is set by the following parameters:

- N, the number of $B^0\overline{B}^0$ events, which for a luminosity of $3 \times 10^{33}\mathrm{cm}^{-2}\mathrm{s}^{-1}$ and 2 years of running is $N = 6 \times 10^7$.
- B, the branching ratio for the CP mode. For ψK_S^0, $\psi \to \ell^+\ell^-$, this is about 5×10^{-5}.
- ϵ_c, the efficiency for observing the decay $B \to f_{CP}$. For ψK_S^0, $\epsilon_c = 0.51$.
- ϵ_t, the effective tagging fraction. $\epsilon_t = \epsilon_{tag} D^2 = 0.34$.
- f, a factor which takes into account the ratio between the average asymmetry, averaged over the mixing oscillation, and the maximum value. This is about 0.5, close to the value for perfect vertex resolution.

From these, one can estimate the error in $\sin(2\beta)$:

$$\delta[\sin(2\beta)] = \left[N \epsilon_c \epsilon_t f^2\right]^{-1/2}. \tag{1}$$

The factor D in the formula for effective tagging efficiency can also be represented as $1 - 2w$, where w is the fraction of tags which have the wrong sign. This is often called a dilution factor, which is confusing because it takes the largest value of one for perfect tagging. It is better to think of it as a tagging polarization parameter, $D = (R - W)/(R + W)$, where $R(W)$ is the number of right(wrong) sign tags. Then the measured asymmetry is just $A_m = D \times A_0$, where A_0 is the asymmetry that would have been seen with perfect tagging. This is analogous to the effect a spin polarization parameter has on a parity-violating asymmetry.

For each event, all available information is used to calculate a combined tagging factor. In most events, at least one tagging indicator is available, and in many events more than one is. The combined tagging factor is then used to calculate an effective tagging efficiency $[\epsilon D^2]_{eff}$. Table III shows the effective tagging efficiency.

Class	Effective efficiency $[\epsilon D^2]_{eff}$
primary leptons	0.13
all other tags	0.21
All	0.34

Table III: Tagging Performance

The resolution on the CP-violating phase $(\phi_M - \phi_D)$ obtained with an integrated luminosity of 30 fb^{-1} for each CP state is given in Table IV. The combined sensitivity for $\sin 2\alpha$ and $\sin 2\beta$ is estimated to be ± 0.059 and ± 0.085, respectively. The channels $J/\psi K^*$, D^*D, D^*D^*, $\rho\pi$, and $a_1\pi$, which are not pure CP eigenstates, are assumed to be dominated by a single CP eigenstate.

Figure 13 shows a speculation about what the status of the allowed region for the unitarity triangle might be in four years, using non-CP-violating measurements on Bs together with ε from $K_L \to \pi^+\pi^-$. I assume reasonable improvement in experimental measurements and in lattice gauge calculations of hadronic matrix elements. The bands correspond to 1.5 standard deviation contours.

Figure 14 shows the effect of the CP measurements with BABAR in one year of running, also using 1.5 standard deviation limits. This would represent a decisive test of the standard model origin of the CP violation that we already observe in the K^0 system. Some of the many other explanations would predict these asymmetries to be zero on this scale, or dramatically different from those shown here.

CP State	Br	$\phi_M - \phi_D$	$\sigma(\sin(2\phi)$
$J/\psi K^0_S$	0.5×10^{-3}	β	0.098
$J/\psi K^0_L$	0.5×10^{-3}		0.16
$J/\psi K^*$	1.6×10^{-3}		0.19
D^+D^-	6×10^{-4}	β	0.21
$D^{*+}D^{*-}$	7×10^{-4}		0.15
$D^{*\pm}D^{\mp}$	8×10^{-4}		0.15*
Combined		β	0.059
$\pi^+\pi^-$	1.2×10^{-5}	α	0.20
$\rho\pi$	5.8×10^{-5}		0.11
$a_1\pi$	6×10^{-5}		0.24*
Combined		α	0.085

Table IV: Error on the measurement of $2(\phi_M - \phi_D)$ from various channels for $30\,\mathrm{fb}^{-1}$ (one Snowmass year at design luminosity).

5 Conclusions

I can best summarize the talk with a series of conclusions.

- The experimental signature of the Kobayashi-Maskawa explanation of CP-violation is the existence of large, predictable asymmetries in the decays of the B^0 meson.
- Measuring these asymmetries with good precision in many modes is the primary goal of the Asymmetric B-Factories under construction at SLAC and KEK.
- The PEP-II project is on schedule to obtain collisions in mid-1998.
- This scientific opportunity has attracted a strong international collaboration that has designed the *BaBar* experiment.
- The *BaBar* experiment was approved by the laboratory and by DOE and other funding agencies in recent months. The construction schedule leads to first physics data in early 1999.
- We look forward to being an important part of an upcoming golden era in heavy quark physics throughout the world of high energy physics.

I acknowledge the efforts of the many members of the *BaBar* collaboration who contributed to the Technical Design Report, from which the material for this talk was drawn. Jonathan Dorfan provided material on the PEP-II status.

References

[1] "An Asymmetric B Factory Based on PEP", The Conceptual Design Report for PEP-II, SLAC-372 (1991).

[2] "*BaBar* Technical Design Report", SLAC-R-95-457 (1995).

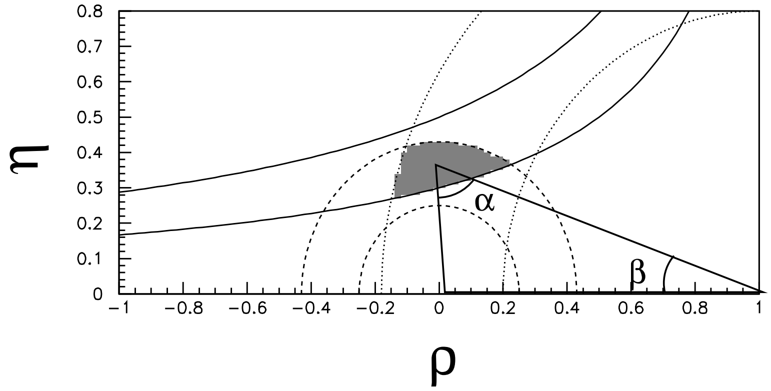

Figure 13: A speculation about the allowed region in $\rho - \eta$ space that might apply in 1999. The triangle is an example of an allowed CKM unitarity triangle. The angles α and β are the CP angles measured at PEP-II.

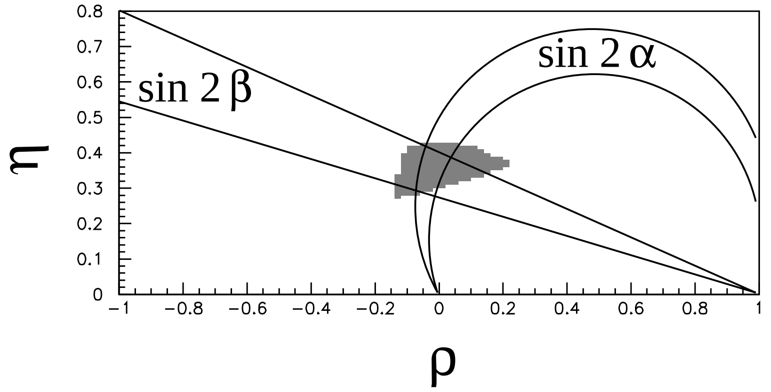

Figure 14: A similar plot, showing the allowed region from figure 13 along with the constraints from the measurements of $\sin 2\alpha$ and $\sin 2\beta$ in one year of running at the PEP-II design luminosity.